FINAL TECHNICAL REPORT

AWARD# 04HQGR0024

TITLE: CONSTRAINTS ON LATE PLEISTOCENE AND ACTIVE UPLIFT RATES ALONG THE SERRA FAULT AND THE TIMING OF LATE PLEISTOCENE TRANSPRESSIONAL DEFORMATION ALONG THE SAN ANDREAS FAULT, NORTHERN SAN FRANCISCO PENINSULA

Principal Investigators / Authors:

S. John Caskey, Department of Geosciences, San Francisco State University, San Francisco, CA 94132; phone: 415-405-0353; fax: 415-338-7705; e-mail: caskey@sfsu.edu

Karen Grove, Department of Geosciences, San Francisco State University, San Francisco, CA 94132; phone: 415-338-2617; fax: 415-338-7705; e-mail: kgrove@sfsu.edu

Chimi Li, Department of Geosciences, San Francisco State University, San Francisco, CA 94132

Glenn W. Berger, Desert Research Institute, 2215 Raggio Parkway, Reno, NV 89512.

Program Element: I

Research supported by U.S. Geological Survey (USGS) Department of the Interior, under USGS award number 04HQGR0024. *The views and conclusions contained in this document are those of the authors and should not be interpreted as necessarily representing the official policies, either expressed or implied, of the U. S. Government.*

AWARD# 04HQGR0024

TITLE: CONSTRAINTS ON LATE PLEISTOCENE AND ACTIVE UPLIFT RATES ALONG THE SERRA FAULT AND THE TIMING OF LATE PLEISTOCENE TRANSPRESSIONAL DEFORMATION ALONG THE SAN ANDREAS FAULT, NORTHERN SAN FRANCISCO PENINSULA

Principal Investigators / Authors:

S. John Caskey and Karen Grove (P.I.'s), Department of Geosciences, San Francisco State University, San Francisco, CA 94132; phone: 415-405-0353; fax: 415-338-7705; e-mail: caskey@sfsu.edu and kgrove@sfsu.edu

Chimi Li, Department of Geosciences, San Francisco State University, San Francisco, CA 94132

Glenn W. Berger, Desert Research Institute, 2215 Raggio Parkway, Reno, NV 89512.

TECHNICAL ABSTRACT

The objectives of this project were to complete the study we previously initiated to document the style and rates of uplift along the Serra fault, and the timing of the onset of transpressional tectonics in southwest San Francisco. The funds were primarily used to support Chimi Li's MS research on the sedimentology of the Colma Formation near Fort Funston and to date Colma fromations sediments at key stratigraphic positions using thermoluminescence (TL) and optically stimulated luminescence (OSL) dating techniques, which are optimal for the types of deposits and general age ranges that characterize the units. Although we succeeded in our efforts to better characterize the sedimentologic chraracteristics of the Colma Formation showing that the Colma Formation at Ocean and Thornton Beaches was deposited in a beach environment. Because these exposures are currently located from ~25 m to ~70 m above present day sea level, the sediments have been uplifted to their current elevations, principally by movement along the nearby Serra thrust fault. The OSL analyses for these sediments yielded ages far younger than previously proposed ages for the Colma and far younger ages than are reasonable for Colma Formation. Based on geologic relations and knowledge of the history of sea-level fluctuations along the California coast, our currently preferred ages for the uppermost sequences of the Merced Formation and the Colma formation are as follows: 1) ~200 or ~300 ka for the Merced X-Sequence; 2) ~120 or ~200 ka for the Merced Y-Sequence; and 3) ~83 or ~120 ka for the Colma Formation. An angular unconformity represented by the XY boundary of the Merced Formation appears to mark the onset of folding along the northernmost, blind expression of the Serra fault near Fort Funston. Our preferred age estimates for the Colma Formation suggest uplift rates associated with deformation along the Serra fault system of 0.5-1.0mm/yr at Thornton Beach and 0.2-0.5 at Ocean Beach.

FINAL TECHNICAL REPORT—

TITLE: CONSTRAINTS ON LATE PLEISTOCENE AND ACTIVE UPLIFT RATES ALONG THE SERRA FAULT AND THE TIMING OF LATE PLEISTOCENE TRANSPRESSIONAL DEFORMATION ALONG THE SAN ANDREAS FAULT, NORTHERN SAN FRANCISCO PENINSULA

INTRODUCTION

The objectives of this project were to complete the study we previously initiated to document the style and rates of uplift along the Serra fault, and the timing of the onset of transpressional tectonics in southwest San Francisco. The funds were primarily used to support Chimi Li's MS research on the sedimentology of the Colma Formation near Fort Funston and to date Colma fromations sediments at key stratigraphic positions using thermoluminescence (TL) and optically stimulated luminescence (OSL) dating techniques, which are optimal for the types of deposits and general age ranges that characterize the units. Although we succeeded in our efforts to better characterize the sedimentologic chraracteristics of the Colma Formation showing that the Colma Formation at Ocean and Thornton Beaches was deposited in a beach environment. Because these exposures are currently located from ~25 m to ~70 m above present day sea level, the sediments have been uplifted to their current elevations, principally by movement along the nearby Serra thrust fault. The OSL analyses for these sediments yielded ages far younger than previously proposed ages for the Colma and far younger ages than are reasonable for Colma Formation. Below we summarize the results of our sedimentologic studies and interpretations regarding the most likely ages for late Pleistocene sediments (uppermost Merced and Colma formations), and uplift rates along the northernmost expression of the Serra thrust fault. Unfortunately the OSL ages obtained from these units as well as several other marine terrace units along this same area of the coast are inaccurate. The most likely cause is the presence of un-removed feldspar grains in the samples, or of feldspar micro-inclusions within the quartz grains. Repeat sample purification and IR tests are being carried out at DRI. Presentation and discussion of the analytical results from the OSL-dating are included as Appendix I.

METHODS

We conducted field work at two locations: Ocean Beach, between Sloat Boulevard and Fort Funston, and Thornton Beach (Fig. 2). Before starting field work, I obtained a research and collecting permit from the National Park Service that allowed for low-impact research and sampling of the Colma and uppermost Merced Formations. During field investigations I measured detailed stratigraphic sections to reassess depositional environments, examined structural features, and sampled for grain size analysis and optically-stimulated luminescence (OSL) dating (Aitken, 1998). OSL samples were taken in January, 2004, and the bulk of the field work took place from June to October, 2004.

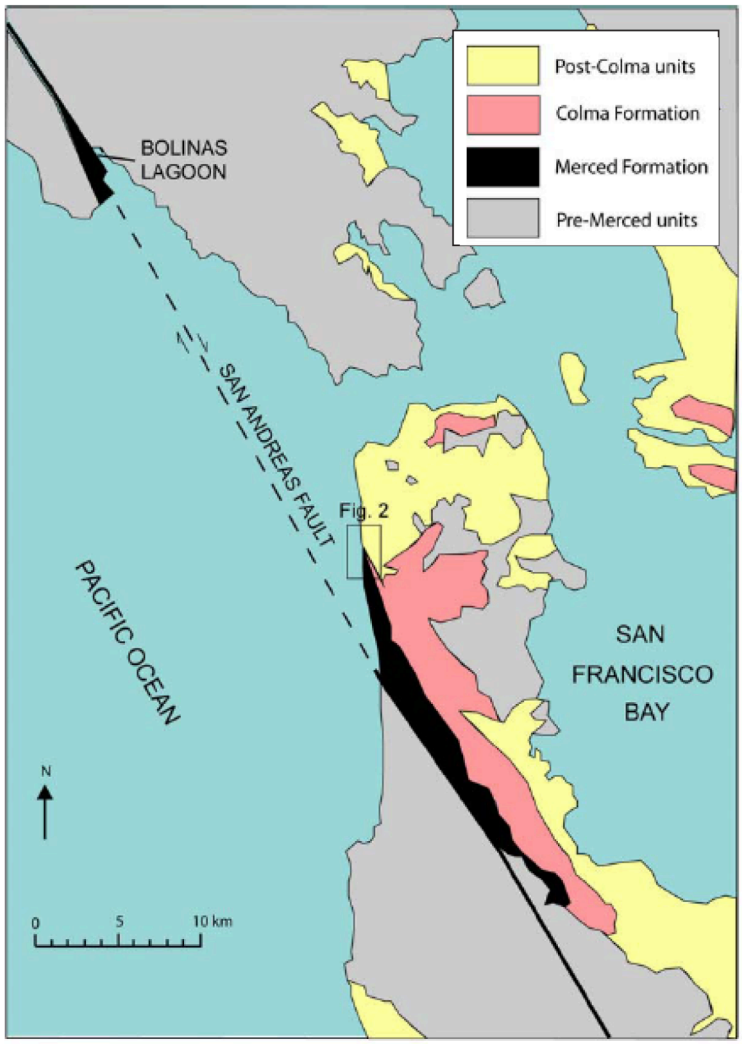

Figure 1. Map of San Francisco Peninsula and areas to the north, showing distribution of major exposures of the Colma and Merced Formations and both older and younger units. (Adapted from Clifton and Hunter, 1999)

Stratigraphic Investigation

Stratigraphic columns were constructed for the Colma and uppermost Merced Formations, and associated channel-fill deposits, where the units are most completely exposed (Li, 2005). At Ocean Beach, a ~20-m-thick section of the Merced Y-Sequence is exposed in the sea cliffs, from just south of Sloat Boulevard to just north of Fort Funston (Figure 2). Near Sloat Boulevard, only the upper beds of the Y-Sequence are exposed in the cliffs. To the south, the sequence dips more steeply and a thicker section is exposed. During the period of field work, the base of the sequence was not accessible at beach level, as debris cones had built up along the beach at the cliff base. For the stratigraphic column of the Merced Y19 Sequence, Li (2005) measured the base at the lowest elevation where it was exposed in the cliffs, about 7–8 m above beach level (Figure 3). The sequence was examined in roughly 0.1 m increments.

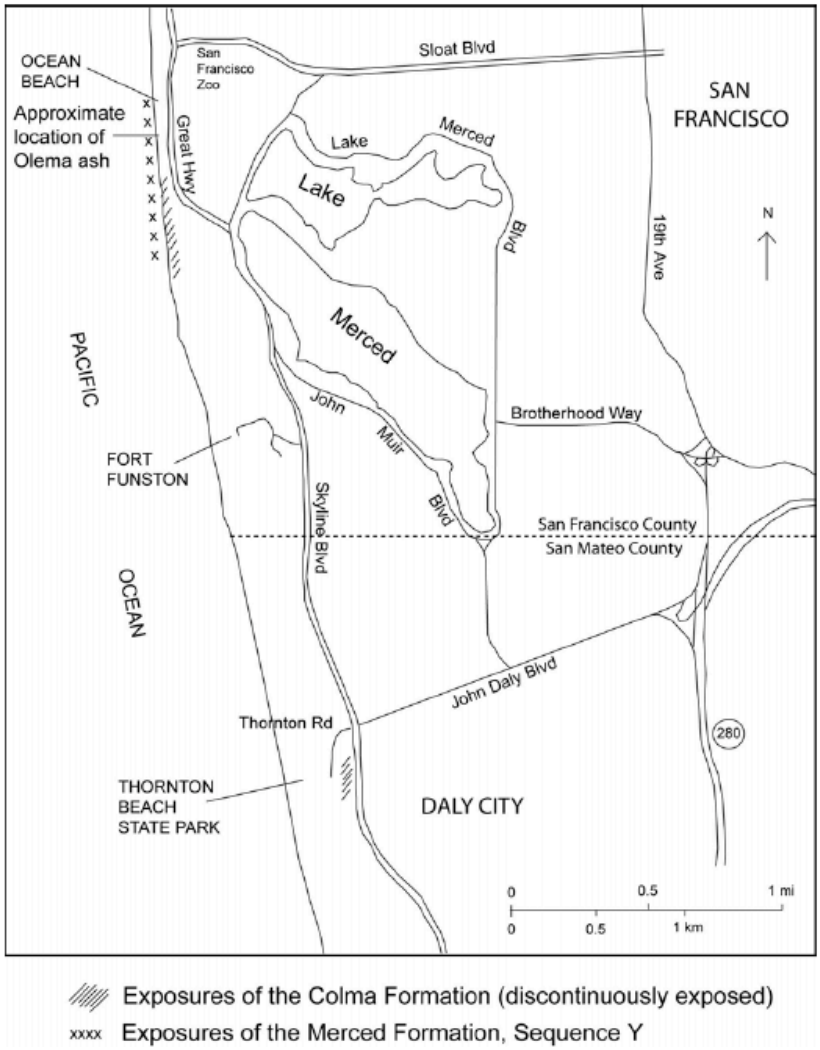

Figure 2. Ocean Beach and Thornton Beach location map, showing the approximate extents of exposures of the Colma and uppermost Merced formations. Exposures of the Colma Formation at Thornton Beach are about 30-50 m higher in elevation than the Ocean Beach exposures. (Adapted from Clifton et al., 1988)

At Thornton Beach, an 11–12-m-thick section of the Colma Formation is exposed in an eroded drainage gully just off of old Thornton Road (Figures 2 and 3), which was abandoned years ago because of landsliding. During the course of this study, the upper part of the road was graded and turned into a parking lot and vista point. The top ~8 m of this deposit can be correlated to another, topographically higher exposure that is located roughly 100 m south along the old road. The bottom few meters of the road exposure have been obscured by road development. It is possible that the gully exposure is a topographically lower section of the Colma Formation that is continuous with the road exposure. However, because landsliding has occurred at this location, the gully exposure is most likely a slump block resulting from landslide activity. Stratigraphic section thicknesses were measured with a tape measure and Jacob staff to measure. Depositional environments were inferred from sedimentary structures in the stratigraphic sequences

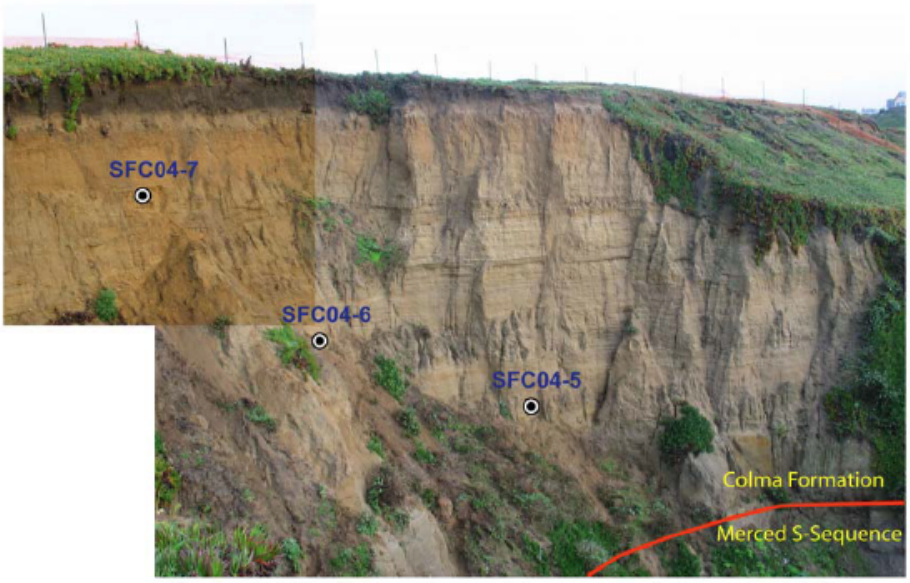

Figure 3. Sea cliff exposure of the Colma Formation at Thornton Beach (gully exposure), showing OSL sample site SFC04-5, SFC06-6, and SFC04-7, and contact (red line) with underlying Sequence S of the Merced Formation (Hunter and Clifton, 1982).

and comparisons to characteristics of present day coastal depositional environments described by Clifton et al. (1971) and Hunter et al. (1984). A generalized stratigraphic columns for the Colma Formation at the Thornton Beach study area, including OSL sample locations are provided in Figure 5. Detailed stratigraphic columns for this study can be found in Li (2005).

Optically-Stimulated Luminescence Dating

Luminescence dating of unheated sediments is able to produce ages up to at least 500 ka by measuring acquired nuclear radiation in silicate minerals (Aitken, 1985; Berger, 1994; Aitken, 1998; Forman et al., 1998). There are two main techniques involved in luminescence geochronology: thermoluminscence either technique, it is necessary to collect sediments behind the outcrop surface, to avoid weathered sediments and exposure to sunlight (Aitken, 1998; Forman et al., 1998). The TL signal in silicate minerals consists of a light-insensitive and light-sensitive component. The light-sensitive component is assumed to be reduced to zero when the sediments are fully exposed to sunlight prior to subsequent deposition and burial. After burial, it is replenished by low-level background radiation in the sediments at a constant rate (Berger, 1995). Heating the sediments in the laboratory releases both the light-sensitive and lightinsensitive charges and, with suitable correction, gives a TL signal proportional to post-depositional radiation dose. This is then translated to age using a calibrated laboratory radiation dose rate. OSL is similar to TL, except that light of a particular wavelength range is used to stimulate the release of only the lightsensitive charges from the minerals (Aitken, 1998). The OSL clock is considered better suited for coarser grains such as coastal sand because it is more readily zeroed than the TL clock (Aitken, 1998), and is, therefore, the technique used to date my samples. All OSL work was done in collaboration with Dr. Glenn Berger of the Desert Research Institute (DRI), Reno, Nevada, using the single-aliquot regenerative-dose (SAR) protocol described in Murray and Olley (2002).

OSL sample collection

We collected seven samples for OSL dating in January 2004. Each sample was collected in one to three, 8-ounce, light-tight metal tins. Three smaller, 1-ounce sub-samples were taken above, at, and below each OSL sample location, for analysis of environmental parameters such as water content and gamma-ray dose rate. We collected six of the samples from freshly exposed cliff faces by first scraping off the surface sediments and taking the sample 15– 50 cm horizontally behind the surface. One sample (SFC04-4) was collected 50 cm below the surface in a small pit that we dug into the top of a cliff.

OSL laboratory procedures

Laboratory analysis of the samples at DRI began in April 2004. The adapted SAR protocol determines age based on the OSL signals released by multiple quartz grains per aliquot. Before the samples could be measured for OSL signals, they were put through a rigorous sand-quartz sample preparation procedure, which isolates quartz grains of the 105–185 μm size fraction. The procedure requires that the samples be washed first in 1N HCl and then in 30% H_2O_2, to remove any carbonates and organic matter. Samples were then sieved into the 105–210 μm size fraction, and strongly magnetic minerals were removed by a hand magnet. After removal of magnetic grains, the samples were etched in 10% HF acid for 40 minutes, followed by a dionized (DI) water rinse, and were etched in 48% HF for 1 hour, again followed by a DI rinse and a final HCl rinse. This procedure preferentially destroys free feldspar grains (Aitken, 1998). Finally, the samples were sieved into the 105-185 μm size fraction. Unirradiated aliquots of these processed samples were put through an infrared (IR) stimulation test at room temperature, with detection at ca. 410 nm, the peak emission of most feldspars. If a sample failed this IR purity check, it was put through the HF etching procedure again. If a sample passed the second IR test, it moved onto a SAR sample sensitivity test.

The SAR sensitivity test provided estimates for laboratory applied dose rates that were subsequently employed in a full dating SAR experiment. On average, thirty aliquots (ca. 50 grains per aliquot using a 1-mm-diameter disc, or ca. 200 grains per aliquot using a 2-mm-diameter disc) were used in each full dating SAR experiment, with each aliquot usually yielding one paleodose value.

A resultant histogram of SAR paleodose values was then interpreted by Berger to yield a pooled paleodose value for age calculation. This paleodose value was divided by a calculated dose rate to yield a numerical age estimate in calendar years. The dose rate was calculated using updated equations from Berger (1988), adapted to sand-size quartz grains (Aitken, 1998), which incorporated values for K_20 concentrations, U and Th thick-source-alpha-particle counting (TSAC; Huntley and Wintle, 1981), and estimates of past water concentration and a small (usually <5%) cosmic-ray dose rate (Aitken, 1998).

RESULTS

Sedimentology of the Colma Formation (Ocean Beach – Fort Funston Locality)
The exposure of the Colma Formation at Ocean Beach (Figure 4) is a roughly 1-m-thick erosional remnant that unconformably overlies the Merced Formation. Younger dune sand deposits overlie these Colma deposits. The basal contact with the Merced Formation was not observed in the cliff-top OSL sampling pit although it was clearly visible on the cliff face from the beach. The bottommost observable sediments contain scattered, rounded cobbles. Immediately above is a roughly 75-cm-thick sequence of oxidized, horizontally-bedded sand containing heavy mineral laminations and several pebble-sized, angular clay. A few thin, clay lenses and lenses of relatively coarser-grained sand are also present throughout. The sand beds dip less than 5° E. Sand from this exposure is predominantly medium grained.

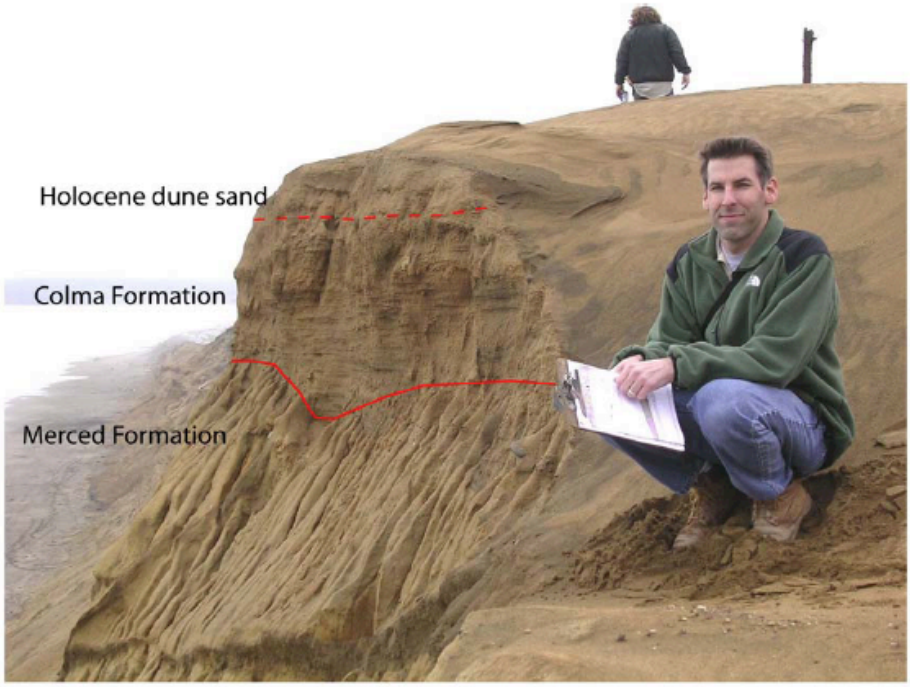

Figure 4. The approximately 1-m-thick erosional remnant of the Colma Formation capping the sea cliffs near Fort Funston at Ocean Beach. The exposure unconformable overlies the Merced Formation along an angular unconformity (solid red line) and is overlain by Holocene and modern dune sand.

The Ocean Beach exposure of the Colma Formation (Figures 2 and 4) was most likely deposited in a foreshore environment, although it could also have been deposited in the backshore. The sediments display heavy mineral laminations that are characteristic of the swash zone. The cobbles below the foreshore sediments may represent a lag deposit, as these sediments directly overlie backshore sediments of the Merced X-Sequence, but cannot be confidently interpreted as such. Because this exposure is an erosional remnant, it is unclear how the stratigraphy of this deposit correlates to the Colma Formation at Thornton Beach.

Sedimentology of the Colma Formation (Thornton Beach Locality)

The exposure of the Colma Formation at Thornton Beach is 11–12 m thick (Figures 3 and 5). Because most of the layers and sedimentary structures present in this sequence are on a cm scale, we describe groups of layers that have similar depositional characteristics rather than describe every individual layer. We refer to each group by a unit number, sequentially designated, starting with the basal unit.

At the Thornton Beach locality, the Colma Formation unconformably overlies S-Sequence sediments of the Merced Formation (Figure 3; Clifton et al., 1988). At the time of this study the contact between these two units was clearly visible in an eroded gully. The underlying light-gray Merced unit is hard and consolidated, whereas the Colma sand above it is yellowish brown to yellowish orange and poorly consolidated. The basal unit (Unit 1) of the Colma Formation is a 3-m- thick deposit of well-sorted, fine- to medium-grained sand.

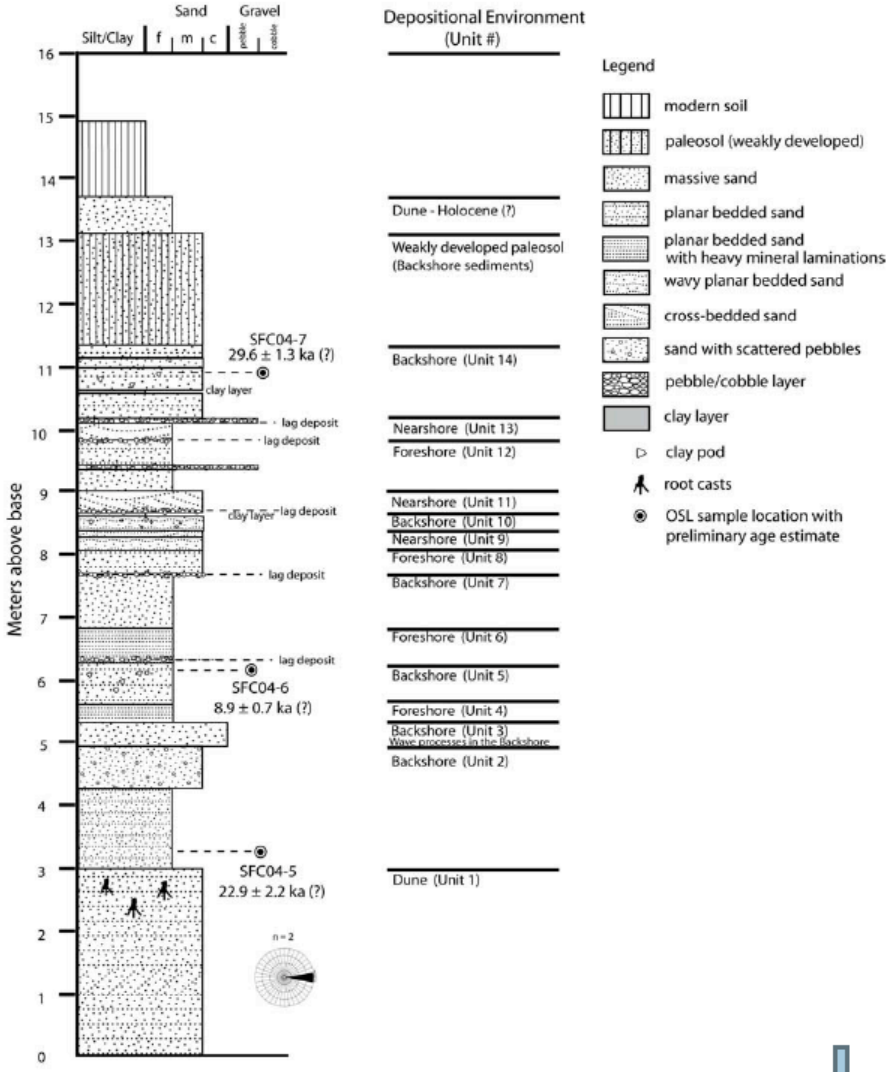

Figure 5. Measured stratigraphic column of Colma Formation sediments at Thornton Beach (Figures 2 and 4). (from Li, 2005).

thick deposit of well-sorted, fine- to medium-grained sand. Just above the base, there are pebble-sized, rounded, clay clasts and sand clasts held together by clay. The sand clasts are probably pieces of the underlying Merced Formation.

Faint planar to wavy bedding is present near the base, and about 0.5-m-thick cross bedding is found farther up section. The cross beds dip eastward (44° to S 85° E and 33° to N 80° E). Thin clay layers are present on top of the cross beds and small, rounded clay clasts are present throughout the unit. In the top 1 m of this unit, there are many oxidized root casts in a zone of oxidized sand. Unit 1 is interpreted as a sand dune deposit. The medium-grained, well-sorted sand and large-scale cross bedding support this interpretation. This unit is similar to the coastal eolian dune facies of the Merced Formation, described by Hunter et al. (1984), which is characterized by mostly fine and some medium grained sand, and medium- to large-scale cross bedding with dip directions mainly to the southeast and northeast. Perhaps this was a sand dune in the backshore environment that occasionally collected water on its surface. Dust that settled or accumulated on top of the damp dune surface could have later turned into the thin clay layers, and dust that settled into empty pockets between dunes could have formed the clay clasts. Alternatively, the clay layers and clasts could be illuvial accumulations on top of bedding planes and within cavities in the sand. As described by Hunter et al. (1984), interdune flats experience various surface conditions, alternately being ponded, subaerially exposed but wet, and dry. Streams carrying clay from nearby Franciscan outcrops could also have entered the dune area. Root casts found within the top 1 m of this unit suggest that vegetation grew on top of the sand prior to deposition of the overlying unit.

Unit 1 grades upward into a 1.92-m-thick deposit of dark-yellowish-orange, fine-grained sand that grades upward into a diffuse zone of pebbles within medium-grained sand (Unit 2). The sand is mostly planar bedded with some heavy mineral laminations. Some wavy bedding is present, and coarser-grained sand fills the low areas in the bedding. The pebbles are subrounded to well rounded. Coarser-grained lenses of sand are present throughout the deposit. A 0.43-m-thick layer of coarse-grained sand with no pebbles (Unit 3) overlies Unit 2. Unit 3 transitions upward into a 0.25-m-thick deposit of planar-bedded, fine grained sand with heavy mineral laminations and some coarse-grained laminations (Unit 4). Beds of this unit dip 3–4° to the east. On top of this laminated unit is 0.64 m unit of horizontally-bedded sand with scattered pebbles (Unit 5). Heavy mineral laminations are faint. A thin clay bed, with numerous cobble-sized clay clasts above and below it, overlies the sand.

Unit 2, 3, and 5 deposits are characteristic of the backshore—horizontally and irregularly wavy-bedded sand with some heavy mineral laminations. These units also display some effects of wave or stream processes. Pebbles within Unit 2 could have been carried from the nearshore zone into the backshore by strong waves or during periods of high tides. Alternatively, the pebbles could have been deposited directly as stream outflow from land into the backshore environment. The coarse-grained sand in Unit 3 may represent a period of high tides, when waves could act on the backshore zone. The sequence of backshore deposits formed by Units 2 and 3 is sharply overlain by a thin unit interpreted

as foreshore sediments (Unit 4). This unit is composed of sand with the typical appearance of swash-zone laminations. Because these deposits overlie backshore sediments believed to be affected by high tides, it is possible that their deposition occurred during this high-tide period. Unit 5 represents a return to normal backshore deposition. The transition from dune to backshore deposits is interpreted as a minor transgressive sequence, with periods of high tide during which wave processes acted on the backshore.

A roughly 0.1-m-thick pebble layer lies between Units 5 and 6. Unit 6 is a 0.60-m-thick deposit of horizontally-bedded sand with heavy mineral laminations. There are several thin gravel layers within this deposit, plus a 19-cm-thick diffuse zone of pebbles and clay clasts. Overlying this laminated unit is a 0.8-m-thick deposit of fine sand with no discernable sedimentary structure (Unit 7). There are several thin pebble layers and one very thin clay bed within this unit.

The pebble layer below Unit 6 is interpreted as a transgressive lag deposit. Units 6–7 are interpreted as a thin foreshore to backshore sequence. Sand with typical swash-zone laminations transitions upward into sand with the type of indistinct bedding characteristic of backshore deposits. This foreshore to backshore sequence seems to have been deposited during a period of fluctuating depositional conditions that were probably a result of changes in sedimentary rate and/or tectonic activity. Because these units are relatively thin it is unlikely that sea level could have risen and fallen quickly enough to create this sequence, although the lag may have formed during a gradual sea level rise. A thin pebble layer separates Units 7 and 8. Unit 8 is a 0.3-m-thick deposit of horizontally-bedded sand that contains lenses of coarser grains. Overlying this unit is a 0.32-m- thick deposit containing layers of wavy-bedded, cross-bedded, and flat-bedded sand with heavy mineral laminations (Unit 9). The sand in all bedding types is predominantly medium grained. The cross-bedded layer is 10– 12 cm thick with a dip of 11° toward S 25° E. On top of this laminated unit is a 0.44 m thick deposit of mostly wavy, horizontally-bedded and massive sand, with scattered pebbles and cobbles throughout (Unit 10). Within this deposit is a 6-cm-thick clay-rich zone that is bounded on the top and bottom by thin clay beds. Between the beds, numerous pebble- and cobble-sized clay clasts are present within the bedded sand.

The pebble layer below Unit 8 is interpreted as a transgressive lag deposit. Unit 8 is interpreted as a foreshore deposit because of the presence of coarse-grained sand lenses within horizontally-bedded, fine sand. The cross bedding present in Unit 9 unit was probably formed by a migrating bedform in the nearshore environment. The southeast dip of the cross beds could be the result of deposition by shoaling waves with a southward component of longshore transport. The moderate dip indicates that the cross-bedding was not deposited by fluvial processes, which characteristically form low-angle-dipping beds (Tucker, 1996). Additionally, the base of the cross bed is flat rather than channelized, which further supports a nearshore interpretation. The wavy, horizontally-bedded sand with interspersed pebbles and clay layers of Unit 10 that overlie nearshore deposits seems similar to the pebbly, clay-rich backshore sediments of Units 2 and 5. The transition from a foreshore/nearshore environment to a backshore environment shows a minor regression

at this time.

A thin pebble layer separates the deposits of Units 10 and 11. Unit 11 is a 19-cm-thick cross-bedded sand layer. To the south of the area of stratigraphic examination, the bed thickens to 30 cm. At this location, the cross beds dip 15° toward N 70° E. The base of the cross bed is very flat. Overlying Unit 11 is a 0.82-m-thick sequence that includes massive sand with no discernable sedimentary structure, horizontally-bedded sand with heavy-mineral laminations, and horizontally-bedded sand with laminations exhibiting inverse-size grading (Unit 12). Several thin pebble layers are present throughout the sequence. A thin pebble layer separates Units 12 and 13. Unit 13 is a 0.34-m-thick unit of crossbedded sand with heavy mineral laminations. A 0.05-m-thick layer of cobbles and many small pebbles overlies the sand. The layer of cross-bedded sand continues to the north of the area of stratigraphic examination, and at this location dips 14° NE toward N 25° E. This bed is 12 cm thick. The topmost unit is a 1.15- m-thick sequence of horizontally-bedded sand layers containing coarser-grained sublayers (Unit 14). Faint heavy-mineral lamination is visible in some layers. Several thin pebble layers and one thin clay bed is present in this sequence, as well as a 32-cm-thick zone of sand containing numerous scattered pebble-sized clay clasts.

The pebble layers separating Unit 10 from 11 and Unit 12 from 13 are interpreted as transgressive lag deposits. The sequence of Units 11 to 14 seems to be progradational overall. Medium-scale, moderately-dipping, cross-bedded sand typical of the nearshore is present in Unit 11 and again farther up section in Unit 13. These cross beds display flat bounding surfaces and tangential foresets. Channels that are interpreted as rip-current channels are also present near the cross-bedded layer in Unit 11. These nearshore deposits are separated by Unit 12, which is interpreted as a sequence of foreshore deposits. Heavy-mineral lamination is absent, but the planar-bedded sand shows laminations with inversegrain- size grading. Swash zone deposits characteristically exhibit inverse-size grading in individual sand laminae (Clifton et al., 1971). The higher nearshore deposits (Unit 13) transition into deposits typical of the backshore — horizontally-bedded sand with faintly visible laminations, clay and pebble layers, and scattered clay clasts and pebbles (Unit 14). Overlying Unit 14 is a thick sequence of paleosols and Holocene dune sand.

The stratigraphy of the Colma Formation at Thornton Beach suggests that the sediments were deposited in a beach environment. The exposure contains deposits associated with nearshore, foreshore, and backshore zones repeated several times within its thickness. Although the bottommost, dune-to-backshore sequence is clearly transgressive, the remaining deposits can be grouped into either regressive or transgressive sequences. Accordingly, the sequence stratigraphy can be supported by either an assumption of a subsiding basin or an emerging basin. If the sequences are interpreted as regressive, then deposition would most likely have occurred in a subsiding basin. Conditions necessary for deposition in a subsiding basin are subsidence combined with depositional progradation and a non-changing sea level. Small amounts of episodic subsidence in combination with a constant, relatively fast rate of sedimentation could have resulted in repeated, progradational sequences. If the sequences are interpreted as transgressive, then

deposition would most likely have occurred in an emerging basin. Conditions necessary for deposition in an emerging basin are uplift combined with a rising sea level. Deposition of progressively deeper sediments as the result of a transgressive sea, in combination with episodic uplift, would explain a repetition of transgressive sequences. In both scenarios, it is likely that fluctuating tide levels, such as large waves flooding the backshore during storm-induced high tides, affected deposition on a smaller scale.

Current Elevations of the Colma Formation

At the Ocean Beach locality (Figure 2), the uppermost X- and Y-Sequences of the Merced Formation are exposed at beach level in a northeast-dipping succession that shallows to very gently east-dipping at its northernmost exposure The Merced Y-Sequence rises in elevation from north to south, with the base of the sequence reaching 20 m above sea level at its southernmost exposure. The Colma Formation unconformably overlies both Merced Y- and X-Sequences at this location, at elevations of about 20–25 m.

At the Thornton Beach locality, the Colma Formation unconformably overlies S-sequence sediments of the Merced Formation. The eroded gully exposure of the Colma Formation (from its contact with the Merced Formation to the top of the modern soil layer) is about 15–16 m thick and lies between 52–67 m above sea level. The road exposure of the Colma Formation is located between 62–73 m above sea level.

Relationships between Angular Unconformities and Folding at Fort Funston

Kennedy (2002) mapped a northeast-vergent, monoclinal fold within beds of the uppermost Merced Formation near Fort Funston (Fig. 2), which he interpreted as a fault-propagation fold formed over the blind, northwestern extension of the Serra fault. He recognized three angular unconformities exposed on the sea cliffs at this location, which appear to record the fold growth. The stratigraphically lowest unconformity separates the Merced X- and Y-Sequences. Immediately below the unconformity, bedding surfaces of eolian deposits of the X-Sequence dip 35–45° to the northeast (Kennedy, 2002). Above the unconformity, the nearshore deposits of the Y-Sequence dip more shallowly, about 10° to 30° to the northeast. The angular unconformity is also supported by stratigraphic truncations of a prominent clay layer beneath the unconformity that is only expressed during certain inter-beach conditions, when the modern beach sand is mostly removed. Kennedy (2002) proposed that this angular unconformity records the onset of fold growth and uplift along the Serra fault. A second, well-documented angular unconformity separates the Merced Y-Sequence and the Colma Formation. Beds within the Colma Formation are generally horizontal to gently northeast-dipping. Kennedy (2002) measured dips of 7–12° NE within the Colma deposits near his South Channel location, where beds within the underlying Merced sequences dip up to 63° to the northeast (Kennedy, 2002). Finally, a third angular unconformity separates the Merced Formation and inset South Channel deposits. The channel deposits, assumed to have been originally westward-grading, are now tilted 7° to the east (Kennedy, 2002). These two stratigraphically higher angular unconformities are proposed to reflect continued fold development. The upward shallowing of the bedding dips of Merced, Colma, and channel

deposits supports the idea that progressive northeastward tilting may have occurred as a result of fold development. Kennedy (2002) also observed several shear fractures with offsets within Merced sediments just north of the South Channel and smaller fractures on the forelimb of the northeast-vergent fold at this location. These fractures were interpreted as the result of strain related to fold growth. Other small-scale thrust faults and conjugate sets of fractures are present within the Merced Y-Sequence sediments farther north of the fold location and may also be related to fold growth.

Kennedy (2002) concluded that the folding and progressive northeast tilting of the Merced X- and Y-Sequences, the Colma Formation, and inset mid to late Holocene channel alluvium above the east-dipping fold limb indicated late Pleistocene to recent activity on the Serra fault. Because the Merced X-Y angular unconformity is interpreted to represent the onset of fold growth, the age of the unconformity is needed to determine the timing of uplift along the Serra fault. Knowing the age and depositional environment of the Colma Formation is needed to determine late Pleistocene uplift rates for the Ocean and Thornton Beach areas.

Age data

Seven samples were collected from the Merced X-Sequence, Y-Sequence, and the Colma Formation for OSL dating. Sample SFC04-2 is from the Merced X-Sequence, samples SFC04-1 and SFC04-3 are from the Merced Y-Sequence, and samples SFC04-4 to SFC04-7 are from the Colma Formation. SFC04-4 is from the Ocean Beach locality and SFC04-5, SFC04-6, and SFC04-7 (taken in stratigraphic order from a lower to higher elevation) are from the Thornton Beach locality. Exact sample locations are displayed on Figures 6 and 7. Three additional samples that are not related to this study (SFC04-8, SFC04 11, and SFC04-12) were collected from marine terrace deposits between Montara Beach and Pillar Point, about 30–50 km south of San Francisco. These samples are not described in detail, but their ages are discussed in relation to the strength of the OSL dating results.

The first-result age estimates from OSL dating of the Colma and Merced sediments are listed in Table 1. At the Ocean Beach locality, the stratigraphically lowest sample taken from the top of the Merced X-Sequence yielded an age of 50.4 ka. Ages for the Merced Y-Sequence range from 32.8 ka at the base to 16.5 ka near the middle of the section. The overlying Colma exposure at this Ocean Beach locality yielded an age of 7.5 ka. The Colma samples taken from the Thornton Beach section yielded ages of 22.9 ka near the base, 8.9 ka in the middle of the section, and 29.6 ka near the top.

All OSL ages appear to be much too young when considering available constraints for these deposits. The 50.4 ka age for the Merced X-Sequence and the 16.5–32.8 ka ages for the Merced Y-Sequence are not consistent with the presence of 55–75 ka Olema ash within fluvial deposits inset into the YSequence. The inset relation of the ash into the Y-Sequence requires this sequence to be older than at least 55–75 ka and for the X-Sequence to be older still.

The age of the Colma Formation at Ocean Beach is constrained by the 5.9–7.0 ka fluvial

deposits which are deeply inset into Merced and Colma deposits. The inset relation of the channel deposits into the Colma Formation requires the formation to be older than at least 7.0 ka. The 7.5 ka age result for the Colma deposits at Ocean Beach is therefore possible, but the Olema ashbearing deposits farther north also appear to be inset into a surface capped by the Colma Formation. Thus, it is unlikely that the formation is younger than 55– 75 ka. If the Colma Formation pre-dates the deposition of the ash layer, then the Y-Sequence, accordingly, would be much older than 55–75 ka. A 7.5 ka age for the Colma Formation at Ocean Beach is additionally improbable considering that the sediments appear to be foreshore or backshore deposits that would have required deposition during a paleo-highstand. The 7.5 ka age would tie this exposure to the current highstand of the sea, when the level was about 15 m lower than present day sea level. This age is highly improbable considering that the Colma is located ~25 above sea level and the age would require a 5 mm/yr uplift rate to account for 40 m of uplift since deposition. Along the central coast of California, uplift rates generally range from about 0.2–0.5 mm/yr (McKittrick, 1988; Muhs et al., 1990) and have not been known to exceed 1.1 mm/yr (Perg et al., 2001; Grove, 2003). The OSL ages for Colma sediments at Thornton Beach are difficult to accept at face value because they are out of stratigraphic order. The 22.9 ka age near the base and the 29.6 ka near the top are inverted, and the 8.9 ka age in the middle of the section appears to be much too young. The stratigraphic inconsistence of the age results supports the idea that a sampling or lab error may have occurred. If these Colma deposits are depositionally correlative to the Colma Formation at Ocean Beach (which they appear to be), then it is unlikely that they are younger than 55–75 ka. If Colma deposits from the two locations are unrelated and the older ~22-29 ka ages for the Thornton Beach deposits are correct, improbably large uplift rates are necessary to account for the current elevations of the deposits. The Colma sediments at Thornton Beach are interpreted as a series of nearshore, foreshore, and backshore deposits that would have been deposited during a sea level highstand. The sea level high stands closest to the ~22-29 ka ages, those within the 35–60 ka range (OIS 3), were all 50 m or more below present day sea level (Lambeck and Chappell, 2001). If the Thornton Beach exposures were deposited during one of those highstands, uplift rates of 2–3 mm/yr would be required to account for their present maximum elevation of ~70 m. These uplift rates are two to three times higher than known coastal uplift rates in the San Francisco Bay Area. The ~33-44 ka ages for the marine terrace samples (SFC04-8, SFC04-11, SFC04-12) are also too young when considering previously proposed ages for the terraces based on stratigraphic observations. All terraces from which the samples were taken have been previously correlated to highstands of OIS 5 (~83–120 ka) and most probably even older for the terrace at Montara beach (sample SFC04-12), and are unlikely to be younger than OIS 5a.

In summary, the first-result OSL age estimates for all samples appear to be systematically too young. At the Ocean Beach locality, there is general stratigraphic consistence of the Merced X-Sequence, Y-Sequence, and Colma Formation age results. However, the ages for the Colma Formation at the Thornton Beach locality are inverted, with an anomalously young age in the middle of the section. The apparent erroneous ages for all samples and stratigraphic inconsistence of Thornton Beach samples suggest that a sampling

or lab error may have occurred.

Table 1. OSL SAR Age Results for the Colma and uppermost Merced formations at Ocean Beach and Thornton Beach and marine terrace deposits at Montara Beach and fron near Pillar Point.

LOCATION	CURRENT ELEV. (m)	SAMPLE	OSL AGE (ka)
Modern beach sand, Ocean Beach	0	SFC04-10	0.022 ± 0.009
Colma Fm. (top), Thornton Beach	64	SFC04-7	29.6 ± 1.3
Colma Fm. (middle), Thornton Beach	58	SFC04-6	8.9 ± 0.7
Colma Fm. (base), Thornton Beach	55	SFC04-5	22.9 ± 2.2
Colma Fm., Ocean Beach	25	SFC04-4	7.5 ± 0.6
Merced Fm. (middle of Y-Seq.), Ocean Beach	12	SFC04-1	16.5 ± 1.2
Merced Fm. (base of Y-Seq.), Ocean Beach	9	SFC04-3	32.8 ± 1.1
Merced Fm. (top of X-Seq.), Ocean Beach	7	SFC04-2	50.4 ± 2.4
Montara terrace sequence, Montara Beach	-	SFC04-8	44.2 ± 3.7
Marine terrace, Pillar Point	-	SFC04-11	33.4 ± 1.6
Marine terrace, Moss Beach	-	SFC04-12	34.0 ± 1.6

Preferred Age Estimates for the upper Merced and Colma Formations
The youngest sea-level highstands that the Colma and Merced Y-Sequence can reasonably be correlated to are those at 83 ka (OIS 5a) and 120 ka (OIS 5e). Older ages of 120 ka (OIS 5e) for the Colma Formation and 190–230 ka (OIS 7) for the Y-Sequence are also just as probable. Accordingly, the underlying, shallow-marine sediments of the X-Sequence may correlate to the sea-level highstands of the 190–230 ka interval (OIS 7) or ~300 ka (OIS 9). All suggested age estimates would be consistent with the 55–75 ka Olema ash in channel deposits inset into the Y-Sequence, and additionally, would not conflict with other stratigraphic constraints such as the Rockland Ash within the Merced S-Sequence.

Estimated Uplift Rates for the Colma Formation
Combining elevation data and the preferred age estimates for the Colma Formation yield uplift rates that are reasonable and consistent with coastal uplift rates for this area. Uplift rates generally range from about 0.2–0.5 mm/yr (McKittrick, 1988; Muhs et al., 1990) along the central coast of California. At Fort Funston, the Colma Formation is currently located ~25 m in elevation. The 5a highstand has been reported to have been either 5.5 m (Muhs et al., 1994) or 19 m (Lambeck and Chappell, 2001) below present day sea level. An 83 ka age for the Colma Formation would require a 0.3–0.5 mm/yr uplift rate, to account for about 31–44 m of uplift since deposition. The 5e highstand was about 6 m above present day sea level (Lambeck and Chappell, 2001; Muhs et al., 1994). A 120 ka age for the Colma Formation would require a~ 0.2 mm/yr uplift rate at Fort Funston, to account for about 25 m of uplift since deposition.

Colma deposits at Thornton Beach are currently located at a maximum of ~70 m in elevation. Assuming that the Colma exposures at Thornton Beach correlate to those at

Ocean Beach, an 83 ka age for the uppermost Thornton Beach exposures would require a 0.9–1.0 mm/yr uplift rate to account for about 76–89 m of uplift since deposition. Although this rate is higher than average coastal uplift rates for the area, it is not improbable. Kennedy (2002) calculated an estimated 0.7–0.9 mm/yr late Pleistocene uplift rate at Thornton Beach, using the 55–75 ka age of the Olema ash as representative of the age of the Colma Formation. This uplift rate is higher after it is adjusted to consider the dip geometry of the Serra fault. Kennedy (2002) calculated a 0.9–1.2 mm/yr uplift rate, using an average fault dip of 50°. A 120 ka age for the uppermost Thornton Beach exposures would require a 0.5 mm/yr uplift rate in order to account for up to 64 m of uplift since deposition.

CONCLUSIONS

New stratigraphic examination of the Colma Formation at Ocean and Thornton Beaches suggests that the sediments were deposited in a beach environment. The exposure at Thornton Beach contains deposits associated with nearshore, foreshore, and backshore zones repeated several times within its thickness, and the exposure at Ocean Beach is composed of what is most likely foreshore- or backshore-deposited sediments similar those at Thornton Beach. Because the coastal exposures of the Colma Formation are currently located from ~25 m to a maximum of ~70 m above present day sea level, these sediments have been uplifted to their current elevations. Movement along the nearby Serra fault, a blind thrust fault where it extends into southwest San Francisco, is believed to be responsible for the uplift and deformation of the Colma and uppermost Merced Formations. The angular unconformity that separates the uppermost X- and Y-Sequences of the Merced Formation presumably records the onset of late Pleistocene uplift along the Serra fault, marking the transition between a previously subsidence-dominated tectonic regime to an uplift-dominated regime. Eastward-tilted beds within mid Holocene channel deposits (Kennedy, 2002) at Ocean Beach are believed to be the latest record of movement along the Serra fault. OSL dating of sediments of the Merced X- and Y-Sequences and the Colma Formation yielded age estimates far younger than those proposed by previous studies and that do not agree with existing age constraints. Based on available age constraints and stratigraphic context, preferred ages for these sediments are: 1) ~200 or ~300 ka for the Merced X-Sequence, corresponding to OIS 7 or 9 sea-level highstands; 2) ~120 or ~200 ka for the Merced Y-Sequence, corresponding to OIS 5e or 7 sea-level highstands; and 3) ~83 or ~120 ka for the Colma Formation, corresponding to OIS 5a or 5e sea-level highstands. The ~83 ka age estimate for the Colma Formation suggests late Pleistocene uplift rates of 0.3–0.5 mm/yr at Ocean Beach and 0.9–1.0 mm/yr at Thornton Beach. The ~120 ka age estimate for the Colma Formation suggests late Pleistocene uplift rates of 0.16 mm/yr at Ocean Beach and 0.5 mm/yr at Thornton Beach. These rates are consistent with the coastal uplift rates for the central California coast region. Although the first-results OSL age estimates are not considered valid, what was learned from the process of obtaining the age results, such as possible sources of contamination and error, will help shape further attempts to date these sediments.

REFERENCES CITED

Aitken, M.J., 1985, Thermoluminescence dating: London, Academic Press, 359 p.

Aitken, M.J., 1998, An introduction to optical dating: the dating of Quaternary sediments by the use of photon-stimulated luminescence: Oxford, Oxford University Press, 267 p.

Berger, G.W., 1988, Dating Quaternary events by luminescence, *in* Easterbrook, D.J., ed., Dating Quaternary Sediments: Geological Society of America Special Paper 227, p. 13-50.

Berger, G.W., 1994, Thermoluminescence dating of sediments older than about 100 ka: Quaternary Science Reviews, v. 13, p. 445-455.

Berger, G.W., 1995, Progress in luminescence dating methods for Quaternary sediments, *in* Rutter, N.W. and Catto, N., eds., Dating Methods for Quaternary Deposits: Geological Association of Canada, GEOtext 2, p. 81-104.

Clifton, H.E. and Hunter, R.E., 1999, Depositional and other features of the Merced Formation in sea cliff exposures south of San Francisco, California, *in* Wagner, D.L. and Graham, S.A., eds., Geologic field trips in Northern California; centennial meeting of the Cordilleran Section of the Geological Society of America: California Department of Conservation, Division of Mines and Geology Special Publication 119, p. 89-100.

Clifton, H.E., Hunter, R.E., and Bartow, G., 2004, Geology and ground-water resources of the Merced Formation in the Westside basin of coastal San Mateo and San Francisco counties: Northern California Geological Society, Guidebook, 58 p.

Clifton, H.E., Hunter, R.E., and Gardner, J.V., 1988, Analysis of eustatic, tectonic, and sedimentologic influences on transgressive and regressive cycles in the upper Cenozoic Merced Formation, San Francisco, California, *in* Paola, C. and Kleinspehn, K.L., eds., New Perspectives of Basin Analysis: Springer-Verlag, N.Y., p.109-128.

Clifton, H.E., Hunter, R.E., and Phillips, R.L., 1971, Depositional structures and processes in the non-barred high-energy nearshore: Journal of Sedimentary Petrology, v. 41, p. 651-670.

Forman, S.L., Pierson, J., and Lepper, K., 1998, Luminescence geochronology, *in* Sowers, J.M, Noller, J.S., and Lettis, W.R., eds., Dating and earthquakes: review of Quaternary geochronology and its application to paleoseismology: U.S. Nuclear Regulatory Commission publication, p. 259-287.

Grove, K., 2003, Coastal uplift of the Point Reyes Peninsula north of San Francisco, California: Geological Society of Abstracts with Programs, v. 35, n. 4, p. 20-21.

Hunter, R.E., and Clifton, H.E., 1982, Description of beds exposed at Fort Funston, Golden Gate National Recreation Area, northwestern San Francisco Peninsula, California: U.S. Geological Survey Open-File Report 82-1055, 30 p.

Hunter, R.E., Clifton, H.E., Hall, N.T., Csaszar, G., Richmond, B.M., and Chin, J.L., 1984, Pliocene and Pleistocene coastal and shelf deposits of the Merced Formation and associated beds, northwestern San Francisco Peninsula, California: Pacific Section S.E.P.M. Field Trip Guidebook, p. 1-30.

Kennedy, D.G., 2002, Neotectonic character of the Serra fault, northern San Francisco Peninsula, California [M.S. thesis]: San Francisco State University, 117 p.

Lajoie, K.R., 1996, Northeast Santa Cruz Mountains Thrust/Fold Belt, *in* Jayko, A.S., and Lewis, S.D., eds., Towards Assessing the Seismic Risk associated with Blind Faults, San Francisco Bay Region, California: U.S. Geological Survey Open-File Report 96-267, p. 86-104.

Lambeck, K. and Chappell, J., 2001, Sea level change through the last glacial cycle: Science, v. 292, p. 697-686.

Lanphere, M.A, Champion, D.E., Clynne, M.A., and Muffler, L.J.P., 1999, Revised age of the Rockland tephra, northern California: Implications for climate and stratigraphic reconstructions in the western United States: Geology, v. 27, p. 135-138.

Li, Chimi, 2005, Depositional and deformational history of the uppermost Merced and Colma Formations, southwest San Francisco, San Francisco State University, MS thesis. 137 p.

McKittrick, M.A., 1988, Late Quaternary deformation of marine terraces, Monterey Peninsula, California: Geological Society of Abstracts with Programs, v. 20, n. 3, p. 214.

Muhs, D.R., Kennedy, G.L., and Rockwell, T.K., 1994, Uranium-series ages of marine terrace corals from the Pacific coast of North America and implications for last-interglacial sea level history: Quaternary Research, v. 42, p. 72-87.

Muhs, D.R., Kelsey, H.M., Miller, G.H., Kennedy, G.L., Whelan, J.F., and McInelly, G.W., 1990, Age estimates and uplift rates for late Pleistocene marine terraces; southern Oregon portion of the Cascadia Forearc: Journal of Geophysical Research, B, Solid Earth and Planets, v. 95, p. 6685-6698.

Murray, A.S., and Olley, J.M., 2002, Precision and accuracy in the optically stimulated luminescence dating of sedimentary quartz: a status review: Geochronometria, v. 21, p. 1-16.

Perg, L.A., Anderson, R.S., and Finkel, R.C., 2001, Use of a new ^{10}Be and ^{26}Al inventory method to date marine terraces, Santa Cruz, California, USA: Geology, v. 29, p. 879-882.

Murray, A.S., and Olley, J.M., 2002, Precision and accuracy in the optically stimulated luminescence dating of sedimentary quartz: a status review: Geochronometria, v. 21, p. 1-16.

Perg, L.A., Anderson, R.S., and Finkel, R.C., 2001, Use of a new ^{10}Be and ^{26}Al inventory method to date marine terraces, Santa Cruz, California, USA: Geology, v. 29, p. 879-882.

Tucker, M.E., 1996, Sedimentary rocks in the field, 2nd edition (the geological field guide series): West Sussex, John Wiley and Sons, Ltd, 153 p.

Appendix I.

Interim Report 5/31/2005: (for Dr. John Caskey)
SINGLE-ALIQUOT LUMINESCENCE DATING OF EXPOSED MARINE SAND AT SAN FRANCISCO

Glenn W. Berger, Desert Research Institute, 2215 Raggio Parkway, Reno, NV 89512.
Email: glenn.berger@dri.edu

Introduction

Photonic (or optical) dating (e.g., Aitken, 1998; Berger, 1995) is a sensitive means for dating the last exposure to daylight of detrital grains of eolian sediment, hence their burial time. The particular photonic-dating method employed here (single-aliquot B-PSL, or bluelight photon stimulated luminescence) produces a signal from both quartz and feldspars in the fine-sand-size fraction. Since quartz PSL is more stable, feldspars must be removed. The upper age limit of single-aliquot quartz PSL dating is presently about 150-200 ka for typical sediments.

Samples

Results are reported here for 11 samples collected 27.Jan.2004 by Berger under the guidance of Drs. Caskey and Grove, with the assistance of Ms. Chimi Yi. Samples and locations are listed in Table 1. For each sample, three nearby (vertically bracketing) sub-samples were collected for dosimetry measurements. In this report, the average of the dose-rate parameters for the overlying and underlying sub-samples are reported for "environmental dose rate" calculation, as well as the separate values for the sub-sample adjacent to the luminescence-dating sample. This averaging and associated assigned error accommodate any possible heterogeneity of the material surrounding the luminescence sample within a radius of about 30 cm (the typical range of gamma rays in unconsolidated sediment).

Analytical Techniques

For luminescence work, after chemical treatment with 1N HCl acid (to remove possible carbonates), 6% bleach and 30 % H_2O_2 (to remove organic matter), samples were dry sieved into various fractions. Some attempt to remove strongly magnetic grains was made on the 105-210 :m grains, using a hand- magnet procedure, as such grains could impede the efficiency of subsequent HF acid treatment. HF acid was employed to destroy any feldspar grains, using 10% HF acid for 40 minutes, followed by de-ionized (DI) H_2O rinse, then 48% HF for 1 hr (agitated) and 25% HCl acid rinse before final DI water rinse. The resultant grains were dry sieved again, to prepare the 105-185 :m working fraction for subsequent PSL tests.

For each sample, two 4-mm diameter aliquots of this "quartz" were subjected to IR-PSL readout to test for the presence of feldspar contaminant grains not removed by the preceding HF acid treatments. Only feldspars generally respond to IR stimulation (Aitken, 1998). Those samples that evinced significant IR-PSL signal were passed through the 48% HF acid treatment and subsequent sieving again. For some samples "re-purification" had to be repeated 3 times. Following this sample preparation stage, sets of 25-35 aliquots, grain-mask diameters 2 mm or 4mm depending on results of $ sensitivity tests, were prepared. Also based on these $ sensitivity tests (response of aliquot to laboratory $ doses), a full SAR experiment was designed.

The SAR (single-aliquot-regenerative-dose) procedure followed was that of Murray and Wintle (2003), with some change in the preheating temperature. Both preheating and cut-heat temperatures were maintained for 10 s during the appropriate SAR steps. These SAR

experiments generate a sequence of ratios of PSL signals (L_i/T_i) from variable applied doses ("regenerative" doses) to PSL signals from a constant (small) applied dose (the "test dose"). The ratio is calculated from only the first few seconds of PSL, after subtraction of instrumental and signal backgrounds. When plotted against regenerative laboratory dose, these L/T ratios yield a dose-response curve, onto which is interpolated the ratio L_0/T_0, which is the ratio resulting from the natural sample before an applied regenerative dose. The interpolated intercept is the D_E value, below (e.g., FIG. 1).

A luminescence age $t = D_E/D_R$, where D_E is the so-called "equivalent dose", or sometimes called the paleodose (units Gy, 1 Gy = 100 rads). This is a measure of the post-depositional absorbed ambient ionizing radiation dose, and is derived from luminescence measurements. The term D_R is the effective dose rate (units Gy/ka), and is derived from independent measurements of U, Th, K and water concentration in the dose-rate sub-samples. For U and Th measurements, the thick-source-alpha-particle-counting (TSAC) technique (Huntley and Wintle, 1981) was applied to dried powders of the three sub-samples collected with each PSL sample. K was determined by commercial atomic absorption spectrophotometry. Radioactive secular equilibrium was assumed, an assumption apparently valid for many sandy deposits, excluding some fluvial sediments (e.g., Olley et al., 1996). Lacking detailed independent information, the author estimated the past average water concentration ratio to be the average measured as-collected value for the dose-rate sub-samples. Since the samples were once deeply buried, were perhaps wetter at the day of collection than in the summer months, this assumption seems valid. The saturation values were estimated from a capillary-uptake method. The effect of assuming a saturated water concentration is to make the apparent-age estimate somewhat, but not significantly, older. For example, use of saturated water concentrations would increase the age estimates for samples SFC04-1 and SFC04-2 by 4 and 7 ka respectively, or about 2-4 standard deviations (F). Since the samples are unlikely to have been saturated for significant fraction of their burial history, the author's assumption (to use the as-collected values) seems reasonable.

The ultraviolet (UV) luminescence near the known ~350 nm emission from most quartz (Aitken, 1998) was chosen for detection, which is standard practice in the use of SAR dating. This was also made necessary by the use of a blue-diode (~470 nm) stimulation source. To convert the sample's fossil light to an absorbed-energy equivalent, a calibrated laboratory beta (^{90}Sr-^{90}Y) source mounted in the SAR instrument was employed. Signal was recorded with an automated, high-capacity Daybreak Nuclear Model 2200 reader using an EMI 9235Q photomultiplier tube. Dose-response curves and other data were processed with author-produced software.

Results

Dosimetry data and PSL results are listed in Table 2. Details are listed in the footnotes. Ages are determined by dividing a mean D_E value by D_R. The rationale for interpreting sets of SAR quartz D_E values has been outlined by Olley et al. (1999), and others (Bøtter-Jensen et al., 2003). For non-eolian sediments, usually the cluster of lowest-D_E values gives the last exposure-to-daylight value. Several examples of these sets (plotted as histograms) are given below in the Discussion section.

Discussion

Apart from sample #10, the age estimates in Table 2 are believed to be too young (Caskey and Grove, pers. comm., 2005). Several factors can create age underestimation for SAR

dating of quartz separates. The first three items will lead to underestimation of the paleodose or "equivalent dose" (D_E).

1)--Exposure to light in the field during sampling;
2)--Exposure to light in the laboratory during lab processing;
3)--Overestimation of the dose rate;
4)--Presence of feldspars (either undetected feldspar grains or feldspar inclusions within quartz grains) in the post-acid-etch SAR analyses.

Every precaution was taken during field sampling so that fresh exposures were obtained before sampling. However, as discussed below for sample SFC04-4, it is possible (but not probable) that some younger grains in this sample were reworked into the sample horizon from the surface, prior to sample collection. In the laboratory, the 6-10-mm thick end zones of the cylindrical samples (collected in light-tight tins) that were exposed to light in the field were excluded from processing for SAR analyses. Similarly, the laboratory lighting is of very low energy (wavelengths in the range ca. 500-700 nm) and intensity (varies spatially, < tens of microwatts/cm^2), and samples were exposed for only seconds or minutes per step. These conditions meet or exceed the standard practices for such analyses.

The dose rates were calculated in the standard way for quartz grains (Aitken, 1998). The only obvious factor that could have generated incorrectly high calculated dose rates (hence age underestimates) would be under-estimation of the past average water concentrations. As mentioned above, use of saturation values would increase the age estimates by 20-30%, but saturation values are unlikely to have been retained for a significant fraction of burial time. The most likely source of age underestimation, therefore, is the putative presence of feldspar grains that the rigorous acid-etching treatment and the normal IR purity tests failed to remove and detect. Feldspar grains would normally yield too-low D_E values from the SAR method because all luminescence is recorded in the UV. The UV emissions from feldspars are notoriously unstable (Aitken, 1998; Berger, 1995). Furthermore, if the feldspar grains are present as micro-inclusions within the quartz (e.g., Huntley et al., 1993), then acid etching will not remove them. We have no independent evidence that our samples have such inclusions (the literature is sparse, most samples having feldspar micro-inclusions come from Australia and Russia, and nothing is known to the author and colleagues in San Francisco about the regional quartz micro properties). However, conceivably the samples have feldspar grains that were not detected by the routine IR purity test. This is possible if the feldspar contaminants emit much more strongly in the UV than in the deep blue (ca. 410 nm) used in the routine IR tests, or if the random test aliquots had too few grains to be representative, or if the IR test was too insensitive.

Since these first-result OSL ages were produced, newer IR blue-detection tests at DRI revealed feldspar contamination samples 1, 6 and 10, with lesser contamination likely for the remaining samples. The newer tests used larger numbers of grains per aliquot (ca. 1000), an artificial $ dose (to boost signal), and a high readout temperature (125EC, to boost detectability of feldspars: only feldspars are usually stimulated by IR). Unfortunately, the DRI SAR reader (Daybreak Nuclear Model 2200) suffered serous failures in Feb. 2005 before repeat SAR analyses could be made on these samples.

Nevertheless, in this context it is instructive to discuss briefly the nature of the process of interpreting SAR paleodose values used for age calculation. This discussion illustrates that some indirect evidence already exists for the presence in some samples of either feldspar contaminants or of quartz grains inadvertently exposed to daylight during sampling. The

above arguments suggest that it is feldspar grains, not malignant quartz grains that are present.

The simplest and most relevant way to present SAR paleodose values (each aliquot yields one paleodose value, usually) for interpretation is in the form of histograms. Olley et al. (1998, 1999) have shown that eolian sand yields tight, normally distributed histograms, whereas fluvial and other non-eolian sediments are likely to yield distributions skewed to high paleodose (D_E) values. More refined data presentations, which are beyond the scope of this project's OSL data set, are discussed by Bøtter-Jensen et al. (2003). Figure 2 for modern sample #10 shows a skewed distribution. The horizontal arrow shows the range of D_E values used for calculating a weighted (by inverse variance) mean value for age calculation. This distribution shows that a modern analogue to the coastal sands here contains some grains that were not well exposed to daylight, but that the lower end of the distribution can yield a near-zero age (21"9 yrs for sample 10).

Similarly, sample 4 (Fig. 3) also reveals a skewed distribution, but in this case the selected subset of paleodose values (horizontal arrow) yields an age estimate that is stratigraphically too young at 7.5 ka. Even the maximum D_E value (ca. 66 Gy) would not yield an acceptable stratigraphic age for this sample. In view of the IR-test statement above that this sample (and some others) probably has only a small number of contaminating grains, what could account for this apparently dramatic age underestimation? It is interesting that sample #4 is the only sample collected near the modern surface (ca. 50 cm below). This is certainly within the modern root zone, and it is even conceivable that historic disturbances on and within this surface have mixed younger grains into the sampled horizon. Whether this is probable is open for discussion, but this sample's near-surface location could be an important variable.

The histogram for sample 2 in Figure 4 clearly suggests that at least one aliquot has contaminant feldspar (the lowest, isolated D_E value). Note also that the maximum value (ca. 180 Gy) would only double the age estimate (to ca. 100 ka), still unrealistically young by stratigraphic arguments made elsewhere. Further interpretation of this sample's results must await additional, "higher-purity" SAR analyses. Similarly, the histogram for sample 1 (Fig. 5) suggests that at most, repeat higher-purity SAR analyses would only triple the age estimate (to ca. 50 ka, still too young by other arguments. In concluding this section, it must be said that the above caveats assume that only some aliquots have feldspar contaminants. On the other hand, if all of the first-result aliquots had some such malign grains, then repeat higher-purity SAR experiments might yield paleodose values exceeding the maxima illustrated in these representative histograms. However, an assumption that all the aliquots thus far analyzed have had some feldspar contaminant seems to be equivalent to arguing that the feldspar contaminants must be micro-inclusions within the quartz grains. If this is the case, repeated, "purified" SAR analyses are unlikely to yield "stratigraphically accurate" age estimates.

Conclusions

These results are inaccurate. The most likely cause is the presence of un-removed feldspar grains in the samples, or of feldspar micro-inclusions within the quartz grains. Repeat sample purification and IR tests are being carried out at DRI.

TABLE 1. Luminescence Samples

DRI name	Site	Description
SFC04-10	Ocean Beach at Sloat St.	upper 3-4 cm of modern beach in high wave zone.
SFC04-1	Ocean Beach	Merced Y seq., ~5 m below eroded bench surface.
SFC04-2	Ocean Beach	top of Merced X seq., 50 cm below X-Y contact.
SFC04-3	Ocean Beach	base of Merced Y seq., ~1.5 m above cobble layer.
SFC04-4	near Fort Funston	remnant of Colma Fm., top of X seq., 50-60 cm below modern surface and 48 cm below base of Holocene
SFC04-5	Thornton Beach	1.65 m above highest clay bed in Merced R1 seq., and 28 cm above bioturbated zone, and ~11 m below modern surface.
SFC04-6	Thornton Beach	Colma Fm., ~3 m upsection of #5, ~8 m below modern surface.
SFC04-7	Thornton Beach	Colma Fm., 30 m above #6, ~3 m below modern surface
SFC04-8	Montara Beach	in base of Mont. Terrace seq., 95 cm above boulder lag, 16 cm above pebble gravel, 8-10 m below modern surface.
SFC04-11	Seal Cove bluff	marine sand on wavecut platform on Purisima Fm.
SFC04-12/2	Moss Beach	overlying Purisima Fm., ~5.5 m below upper terrace.

TABLE 2. Dose rates, SAR data, and apparent ages for coastal sand samples.

Sample [a]	Water [b]	K_2O [c] wt.%	C_t [d] $ks^{-1} \cdot cm^{-2}$	C_{th} [d] $ks^{-1} \cdot cm^{-2}$	D_{CR} [e] Gy/ka	Dose rate [f] Gy/ka	Pre/Cut-heat [g] (°C)	D_E [h] (Gy)	Age Estimate [i] (ka)
-10	0.22/0.10±0.03	1.17	0.3716±0.0091	0.144±0.026	0.25±0.03	1.76±0.10	200/180	0.037±0.016(25)	0.021±0.009
-1	0.34/0.09±0.02	1.51	0.3238±0.0084	0.139±0.026	0.09±0.01	2.065±0.074	240/190	33.0±2.1(23)	16.0±1.2
	0.30/ "	1.45	0.319±0.026	0.118±0.020					
-2	0.23/0.09±0.02	1.24	0.2555±0.0081	0.114±0.025	0.04±0.01	1.744±0.076	250/190	84.9±1.8(14)	48.7±2.4
	0.22/ "	1.23	0.327±0.041	0.154±0.027					
-3	0.34/0.10±0.02	1.97	0.2577±0.0065	0.088±0.017	0.10±0.02	2.334±0.076	240/200	74.5±1.2(8)	31.9±1.1
	0.30/ "	1.89	0.218±0.012	0.092±0.015					
-4	0.22/0.10±0.03	1.56	0.5782±0.0091	0.233±0.029	0.20±0.02	2.60±0.11	220/160	19.1±1.3(30)	7.35±0.60
	0.18/ "	1.52	0.520±0.059	0.227±0.032					
-5	0.22/0.10±0.02	1.41	0.2203±0.0059	0.064±0.015	0.05±0.01	1.818±0.068	250/190	40.2±3.6(26)	22.1±2.2
	0.20/ "	1.44	0.275±0.014	0.093±0.024					
-6	0.21/0.13±0.02	1.71	0.2539±0.0078	0.120±0.024	0.07±0.01	2.080±0.073	240/190	17.9±1.3(20)	8.61±0.71
	0.22/ "	1.63	0.326±0.030	0.119±0.021					
-7	0.21/0.09±0.02	1.61	0.3287±0.0091	0.198±0.033	0.13±0.02	2.231±0.078	250/190	64.3±1.9(16)	28.8±1.3
	0.22/ "	1.61	0.345±0.018	0.174±0.020					
-8	0.32/0.15±0.03	1.63	0.1701±0.0060	0.073±0.018	0.06±0.01	1.822±0.078	250/200	77.8±5.7(6)	42.7±3.7
	0.24/ "	1.65	0.206±0.026	0.082±0.015					
-11	0.35/0.11±0.02	1.80	0.2504±0.0077	0.105±0.022	0.08±0.03	2.238±0.080	250/200	72.8±2.1(22)	32.5±1.5
	0.28/ "	1.93	0.291±0.021	0.121±0.020					
-12/2	0.28/0.07±0.02	1.71	0.2231±0.0078	0.099±0.024	0.08±0.03	2.110±0.080	250/200	69.7±2.0(18)	33.0±1.6
	0.30/0.10±0.02	1.57	0.257±0.020	0.114±0.020					

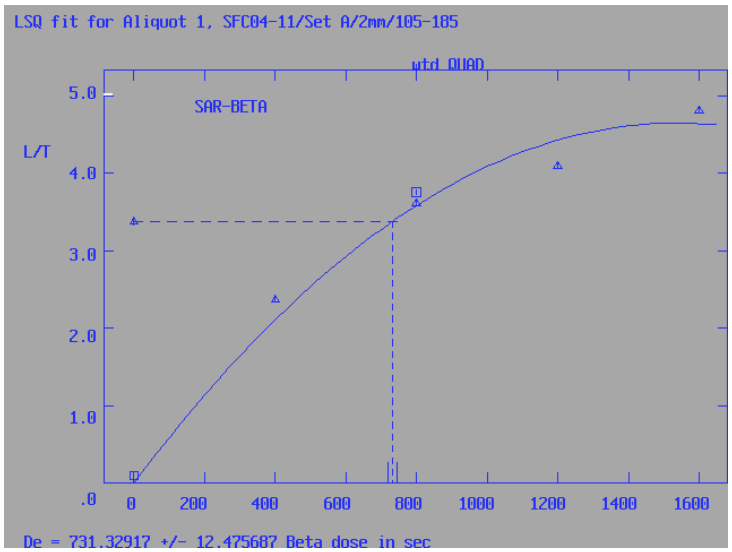

Figure 1. **Regenerative-dose build-up curve of L/T ratios and interpolated L0/T0 ratio (horizontal dash) to yield a De value (SAR method). Two criteria for acceptance of this De value are met here: a "recuperation" L/T ratio near zero (left-hand square) and a "recycling ratio" (ratio of right-hand square to corresponding triangle) near unity.**

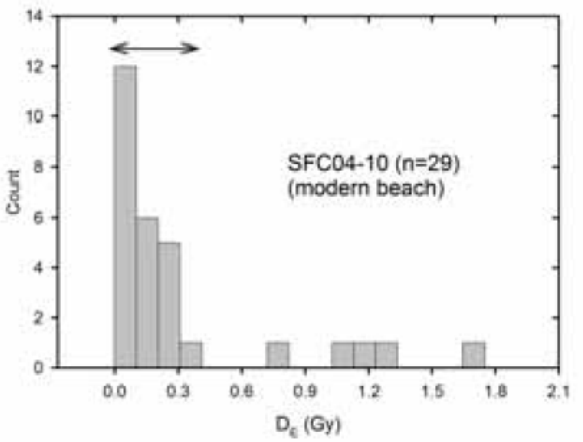

Figure 2.

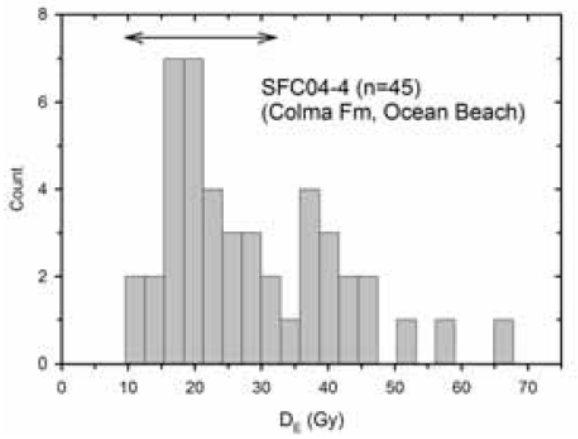

Figure 3.

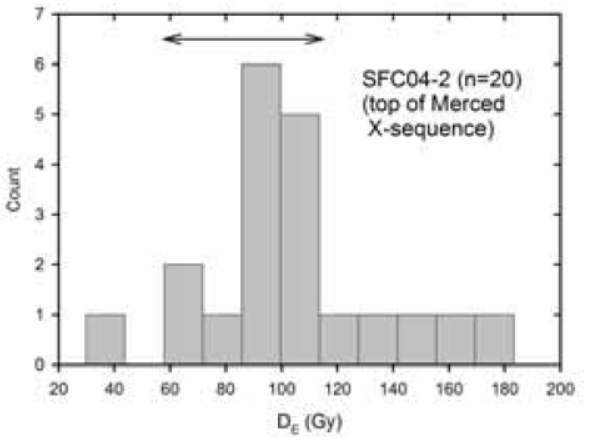

Figure 4.

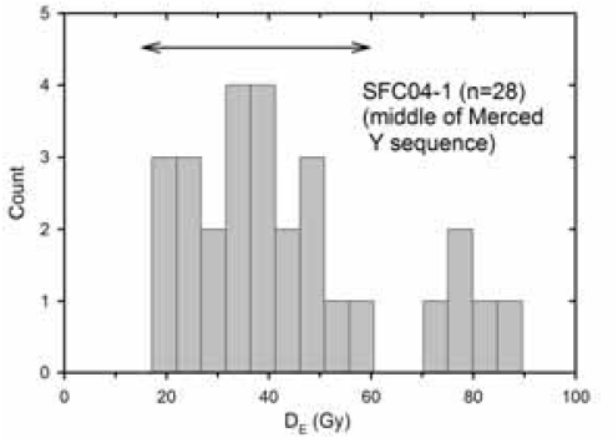

Figure 5.

References

Adamiec, G. and Aitken, M.J. 1998. Dose-rate conversion factors: Update. Ancient TL, v.16, p.37-50.

Aitken, M.J. 1985. Thermoluminescence Dating: Academic Press, San Diego, 351 p.

Aitken, M.J. 1998. Introduction to Optical Dating: Oxford University Press, Oxford, 256 p.

Berger, G.W. 1988. Dating Quaternary events by luminescence, *In* Easterbrook, D.J., ed., Dating Quaternary Sediments: Geological Society of America, Special Paper 227, p. 13-50.

Berger, G.W. 1995. Progress in luminescence dating methods for Quaternary sediments. *In* Dating methods for Quaternary deposits. (Rutter, N.W., and Catto, N., eds.). Geological Association of Canada, GEOtext no. 2, 81-103.

Bøtter-Jensen, L., McKeever, S.W.S., Wintle, A.G. 2003. Optically Stimulated Luminescence Dosimetry. Elsevier, New York, 350 pp.

Huntley, D.J., Wintle, A.G. 1981. The use of alpha scintillation counting for measuring Th-230 and Pa-231 contents of ocean sediments, Can. J. Earth Sci., 18, 419-432.

Huntley, D.J., Berger, G.W., Bowman, S.G.E. 1988. Thermoluminescence responses to alpha and beta irradiations, and age determination when the high dose response is non-linear. Radiation Effects. 105, 279-284.

Huntley, D.J., Hutton, J.T., Prescott, J.R. 1993. Optical dating using inclusions within quartz grains. Geology, 21, 1087-1090.

Murray, A.S., Olley, J.M., 2002, Precision and accuracy in the optically stimulated luminescence dating of sedimentary quartz: a status review. Geochronometria, 21, 1-16.
Murray, A.S., Wintle, A.G. 2003. The single-aliquot regenerative dose protocol: potential for improvements in reliability. Radiation Measurements, 37, 377-381.
Olley, J.M., Murray, A.S., Roberts, R.G. 1996. The effects of disequilibria in the uranium and thorium decay chains on burial dose rates in fluvial sediments. Quaternary Science Reviews (Quaternary Geochronology), 15, 751-760.
Olley, J.M., Caitcheon, G.G., Murray, A. 1998. The distribution of apparent dose as determined by optically stimulated luminescence in small aliquots of fluvial quartz: Implications for dating young sediments. Quat. Sci. Rev., 17, 1033-1040.
Olley, J.M., Caitcheon, G.G., Roberts, R.G. 1999. The origin of dose distributions in fluvial sediments, and the prospect of dating single grains from fluvial deposits using optically stimulated luminescence. Rad. Measurements, 30, 201-217.
Prescott, J.R., Hutton, J.T. 1988. Cosmic ray and gamma ray dosimetry for TL and ESR. Nuclear Tracks and Radiation Measurements, 14, 223-227. 2

[a] DRI sample names are SFC04-nn where “nn” is listed here. The 105-185 :m diameter size fraction of quartz was used for all SAR luminescence measurements. A second row for a sample provides data used to calculate the (dose-rate component (the so-called “environmental” component). 4

[b] Average ratio of weight of water/weight of dry sample. The first number is the measured saturation value, and the second number is the average as-collected value with assigned "1F uncertainty. In the absence of independent evidence suggesting otherwise, this second value is used in the age calculation. Other uncertainties here and elsewhere are reported at "1F.

[c] The estimated uncertainty is "0.05, except for the second row of samples 7, 8 and 11, for which it is "0.06, "0.06, and "0.07 respectively.

[d] Total and thorium count rates from finely powdered samples for thick-source-alpha-particle-counting (TSAC) method (Huntley and Wintle, 1981). $C_u = C_t - C_{th}$. These values are inserted directly into the age equations of Berger (1988), with the internal dose-rate components set = zero.

[e] A cosmic ray component estimated from the algorithm of Prescott and Hutton (1988) (basically, a function of burial depth).

[f] Calculated with the conversion factors given by Adamiec and Aitken (1998), using the equations of Berger (1988). Attenuation of $ rays across the average grain size of 145 :m is accounted for by using attenuation factors of 0.945 for K, 0.875 for U and 0.82 for Th (Aitken, 1985). An estimated small internal dose-rate in quartz of 0.06"0.03 Gy/ka (Murray, pers. comm., 2004) is added to the calculated dose rate.

[g] For the SAR approach, preheat/cut-heat temperatures (Murray and Wintle, 2000), held for 10 s. A signal-readout temperature of 125EC was employed.

[h] The weighted mean plus standard error of the mean for the number of aliquots shown in parentheses.

[I] D_E divided by dose rate.